16th ICAAR
LISBOA 2020-2022

16th International Conference on
Alkali-Aggregate Reaction in Concrete
Lisboa | LNEC | Portugal | 31 May - 2 June 2022
http://icaar2020-2022.lnec.pt

Investigations on reaction kinetics in solution experiments to prevent the alkali-silica reaction

Gyde Hartmut [1], Frank Schmidt-Döhl [2]

(1) Institute of Materials, Physics and Chemistry of Buildings, Hamburg University of Technology, Hamburg, Germany, gyde.hartmut@tuhh.de

(2) Institute of Materials, Physics and Chemistry of Buildings, Hamburg University of Technology, Hamburg, Germany, schmidt-doehl@tuhh.de

Abstract

An alkali-silica reaction (ASR) takes place between alkali hydroxides from the pore solution of the concrete and the reactive siliceous parts of the aggregates. Since the damaging ASR has still not been mastered completely, there are demands for reliable prevention in civil engineering. There are different internationally applied tests for detecting a potential ASR. Some methods assess the reactivity of the aggregate in a defined concrete mixture. Here, the alkali-reactivity is derived from the reaction-dependent expansion of the standardized sample, while others categorize the aggregate in a petrological way, or by solution experiments. The weaknesses of present testing methods are the duration needed for reliable results and the absence of a consistent test method for unknown aggregates.

The aim of this research at the Hamburg University of Technology is a new test method: a faster method for the classification of an unknown aggregate in regards to its alkali-reactivity. The method is based on the reaction kinetics and the multiparameter analysis of accelerated dissolution experiments of the aggregate. The pH-value, the electrical conductivity and the redox potential are recorded during the reaction of the sample with a 1M potassium hydroxide solution. The acceleration of the reaction is affected by the high experimental temperature and an increase of the surface of the sample.

Characteristics of the type and quantity of the aggregate are determined by significant parameters from the data obtained. In this paper, the new experimental approach and first results are presented and discussed.

Keywords: *alkali-silica reaction; asr testing method; durability; dissolution experiments; kinetics*

1.   INTRODUCTION

1.1   The ASR in current literature

During the ASR, the alkali hydroxides from the pore solution of the concrete and the reactive siliceous phases of the aggregates react to form alkali-silica gel [27]. This gel is able to swell in the presence of water through osmosis [20]. The continuous expansion of the alkali-silica gel leads to expansive strain, which is able to exceed the tensile strain capacity of the concrete [2]. The typical macroscopic damages of the ASR are the formation of clearly visible alkali-silica gel, an irregular crack pattern, and funnel-shaped surface spallings, the so-called "popouts". Microscopically speaking, there is alkali-silica gel in the pores and reaction rims in the grains of the aggregate. [2, 12, 20, 27–29] The detailed chemical reactions have been thoroughly discussed in literature, see [5, 17, 24].

The first damage to a concrete structure caused by the ASR was discovered in the USA in 1940, by Stanton [26]. In Germany, ASR-like damage symptoms were noticed in 1965. In 1974, a first version of a German set of guidelines was created to prevent damaging ASR [27].

The preconditions of an ASR are the presence of alkalis, reactive or amorphous silicon dioxide, and water. The amount and their condition have a great influence on the ASR. The amount of alkalis is controlled in national standards. The reference values for the maximum amount of the alkali oxides in the cement (Na_2O-equivalent) and of the total alkali content from the concrete can be found in national standards [9, 12]. These values are the result of previous research and equivocal limits, and do not consider the possibility of additional alkalis from the environment. Additionally, the amount, reactivity, and size of alkali-reactive parts in the aggregate will influence an ASR. Finally, the permeability of the

concrete, the moisture of the concrete structure and the temperature have an effect on the ASR. [2, 12, 20, 27, 28] Considering these factors, the alkali-silica reactivity of the aggregates is the most reliable approach for controlling or even preventing an ASR. The amount of alkalis in the concrete or from an external source and the humidity cannot be controlled and restricted in an easy and reliable way. Therefore, the best option is the classification of the aggregates into different alkali-reactive groups and the adaption of the cement mixture to the alkali-reactivity of the aggregates [27].

1.2   Current problems and aims of this study

There are different national testing standards for categorizing aggregates for alkali-reactivity [2, 27]. Some test methods use the reaction-dependent expansion of a standardized sample to derive susceptibility to ASR. In the rapid mortar bar test, the alkali-reactivity of an aggregate is derived from the expansion of mortar bars under reaction-accelerated conditions. Most of the rapid mortar bar tests of today come from the South African NBRI test by Oberholster and Davies in 1986 [21]. Variations of it are used in many national standards, such as in the German alkali guidelines of the DAfStb [9] or in the ASTM C1260-14 [7]. The drawbacks of these methods are the implementation time (a ten day minimum) and difficulties in assessing unknown aggregates [25]. Furthermore, there are some differences to the results of other established test methods and in practice [27]. Concrete prism tests with a standard formulation of the concrete mixture are the most reliable testing methods. They are used in ASTM C1293 [6] or the guidelines of the DAfStb [9]. These tests need several months and do not take the actual concrete composition or the possibility of additional external alkalies into account [27]. It is possible to perform the concrete prism test with the concrete composition actually used, in the so-called performance tests. For a meaningful evaluation of these methods, there are too few comparable results available currently [14].

Other test methods inspect only the aggregate itself in a petrological, physical, or chemical way. The petrological investigation is essential, but requires much experience, and it is not able to give a quantitative rating about the alkali-reactivity. Using the physical properties to categorize the aggregate, the grain bulk density could be used as in the DAfStb [9] for flint stone. During chemical investigations, as in DAfStb [9], the aggregate is kept in hot sodium hydroxide for 60 minutes. The amount of dissolved silica and reduction in alkalinity of the storage solution is determined. However, these methods are not usable for unknown aggregates without pre-treatment.

The variety of test methods used and the lack of an international, consistent testing method are a sign of the need for an optimization of the procedure. The limits of the present test methods are the long wait for reliable results and the indirect deduction of potential reactivity, the reliability of the results, the non-applicability to unknown aggregates, the lack of taking external alkalis into account, and the missing possibility for precisely measuring the susceptibility of the aggregate to ASR.

The objective of this research at Hamburg University of Technology (TUHH) is therefore to develop a simple, fast, and reliable classification method, which is able to categorize an unknown aggregate concisely regarding its alkali-reactivity.

With the new test method, which will be presented in the following, the ASR susceptibility of an aggregate is derived by reaction kinetics and multiple chemical parameters. They are determined by dissolution reactions of the aggregates. These dissolution experiments are accelerated by a high temperature (60° C), a high pH-value (of nearly pH 14 via 1 M potassium hydroxide solution (KOH)) and, preferably a large surface of the aggregate. The increase in surface is achieved by grinding the aggregate to powder. During the dissolution of the powdered aggregate, the temperature, pH-value, redox potential and electrical conductivity are measured. The analysis of the time sequences and characteristic stationary points of the values leads to some evaluation criteria. The comparison of these points and the results of the dissolution of questionable aggregates should enable a simple and rapid categorization of unknown aggregates according to their alkali-reactivity.

1.3   Dissolution process

The dissolution of silicates is influenced by their particle size, and their structure, temperature, pH-value, and additional ions in the solution. [4, 10] Futher, it is a reaction catalysed by hydroxide ions [18]. In alkaline solutions, hydroxyl ions first deprotonate the silanol groups (Si-OH) on the surface of the solid [24]. This leads to a predominantly negativly charged surface (Si-O$^-$) and to a decrease in hydroxyl ions in the solution. Further, the siloxan bounds (Si-O-Si) are broken up by the hydroxyl ions. This leads to the dissolution of silicic acid from the solid silica. [5]

Monosilicic acid is a weak acid. Its ionizations constants are $K_1 = 10^{-9.8}$ and $K_2 = 10^{-12.4}$ [11, 16]. Thus, in high alkaline solutions, the monosilicic acid ionizes to its anions $(SiO(OH)_3)^{1-}$ and $(SiO_2(OH)_2)^{2-}$. At a pH of 12.6 these are the most common species of the silicic acid [16, 30]. The equilibrium solubility of dissolved silica depends on the amount of monosilicic acid in the solution. Thus ionization of the mono-acid leads to further dissolution of the solid silica, both reduces the concentration of the hydroxide ions and the pH-value, and is supported by the presence of potassium cations in the solution. [1, 10, 24, 30] Monosilicic acid and its anions are able to condensate to polysilicic acids [15]. The condensation of the predominant species of this solutions releases hydroxide ions [16]. This results in an increase in pH-value. The dissolution rates for crystalline and amorphous silica leads to the assumption that they follow the same reaction pathway, though the dissolution rate of amorphous silica is higher [8, 10]. A lower silica concentration in the solution also leads to slower polymerisation of the mono-acid [3].

For developing a new test method based on dissolution process, the dissolution experiments are performed at the same temperature, the same pH-value and the same conditions of the particular aggregates: only the sample size and the material were changed. The new test method uses the faster and stronger dissolution rate of reactive silica, the related faster condensation of the silicic acid and its anions, and their influence on the pH-value, conductivity and redox potential to deduce the alkali-reactivity.

2. METHODS AND MATERIAL

2.1 Experimental setup

The experimental setup consists of a test container where reaction kinetics and chemical parameters are directly measured. The experimental setup is shown in Figure 2.1. It was first mentioned and precisely described in Osterhus and Schmidt-Döhl [23]. The experimental container (1) is hermetically closable with a lid (2) and has an inner volume of 1100 ml. Both are made of Polytetrafluoroethylene (PTFE) to avoid a reaction with the KOH. There are screwed cable ports (3) installed on the lid to attach the electrodes hermetically. Furthermore, there is one aperture which is closed with a PTFE screw (4) for adding the aggregate without opening the whole lid. The KOH solution is therefore only exposed as briefly as possible to the surrounding air, and the potential for carbonation of the solution is minimized. In the middle of the lid is another aperture for potential future use (5), which is closed in order to prevent gas exchange. A magnetic stirrer (6) for avoiding the sedimentation of the specimen is located at the bottom of the PTFE container.
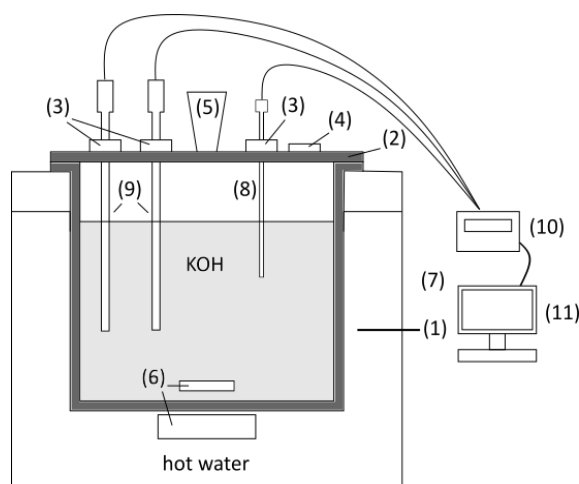

Figure 2.1: Experimental setup

During the experiment, the whole container is heated up in a heat bath with a circulation thermostat, type LAUDA RC20 CP (7). The temperature in the PTFE container is monitored with a PT-1000 sensor by SI Analytics (8). The pH electrode, type H9180, the electric conductivity electrodes, type LF71T1X and LFT1100T+ and the platinum combination electrode for measuring the redox potential, type PT9080 are all made by SI Analytics (9). The electrodes are attached to an eight channel multiparameter device, type C3060 by Consort (10), which passes the data to a computer (11).

2.2 Specimen and test preparation

To increase the surface of the specimen, the aggregates are ground to powder. The aggregate is first roughly ground by a jaw crusher and then pulverized in a planetary mill. For a natural aggregate, several analyses are used to characterize it precisely. The aggregate is weighed to the nearest 0.001 g and stored for 24 hours in an oven at 60 °C.

The 1 M potassium hydroxide solution is made by mixing 56.11 g KOH-platelets with 1 l of distilled water. The KOH-platelets have a purity grade of "pro analysi" (Reag. Ph. Eur.). Their amount of KOH should be at least 85%. The other components, according to the manufacturer's specifications [19], are traces of CO_3, Cl, PO_4 SO_4, Fe and heavy metals.

The pH and redox electrodes are calibrated before every dissolution experiment to prevent measurement errors caused by the considerable abrasion of the aggressive experimental environment. The pH electrode is subject to a four-point-calibration (pH 4, 7, 10 and 13.99). The electric conductivity electrode is tested with the respective standard calibration liquid by SI Analytics. In order to start the experiment, the magnetic stirrer has to be switched on, the KOH solution has to be poured into the PTFE container, the container has to be tightly closed, the electrodes have to be attached to the lid of the container, and the required temperature has to be set on the thermostat. After reaching constant initial conditions of all the parameters, the aggregate is poured in. After 48 to 72 hours, the experiment is terminated. The electrodes are removed and cleaned, and the KOH is disposed of.

2.3 Evaluation of measured data

The pH-value, redox potential, temperature, and electric conductivity are measured and recorded every 30 seconds. The time of adding the aggregate is set as point zero for all measurements. Characteristic points in the data (such as steady states and minima) are identified. The mean and the standard deviation and the variance over comparable experiments of these characteristic points are calculated.

2.4 Material

The chemical composition of the aggregates was determined by XRF spectroscopy with the RFA Horiba XGT-7200 (X-ray tube vol.: 15 kV, XGT diameter: 1.2 mm, process time: 3, current: 1.000 mA, partial vacuum and no filter). The results were analyzed using the fundamental parameter method and the "NIST1881s" reference standard, which was measured with the same conditions as the aggregate. The specific surface was determined according to BET with N_2-sorption with a Micromeritics Accelerated Surface Area and Porosimetry System 2010 (ASAAP 2010). The particle size distribution was measured with a laser diffraction system (Mastersizer 3000 by Malvern) with 1200 rpm in water using ultrasound for breaking up agglomerates, if necessary. The Mie-theory was applied for the analysis of the measurements.

To generate reference data of an aggregate with a high amount of amorphous silica, the experiments were started with Mikrosilica 940 U(SF) by Elkem, hereinafter MS. Reference data of an inert aggregate was generated with quartz powder by Osterhus [22, 23]. Furthermore, two opaline sandstones (OSSN, OSSH) with known alkali-reactivities were examined.

The opaline sandstones were studied, characterized and petrologically analyzed by Franke [13]. OSSH has a density of 1.69 g/cm^3 and was classified as alkali-reactive. OSSN has a density of 1.48 g/cm^3 and was classified as less reactive, see Table 2-1 and Franke [13]. The macroscopic and microscopic investigation did not show any significant differences between both opaline sandstones. The thin sections were investigated by a polarization microscope (Olympus BH2) for a combined reflection and transmission viewing. To determine the crystalline phases, X-ray diffraction was used. The measurements were made by a Philips X'pert Pro MPD diffractometer with Cu-Kα-radiation and the standard software (X'Pert with ICDD file). The major phases of the crystalline structure were identified as quartz, cristobalite, tridymite, opal, mica (muscovite and illite), calcite, glauconite and zeolite. The mineral components are 15 - 20 Vol.-% of opal in form of spicules of sponges and 30 Vol.-% of quartz. The reactivity of opaline sandstone is based on the opal, which constitutes, in this case, 15 to 20 Vol-% of the aggregate. These investigations were omitted for the MS. The results of the chemical and physical properties of the aggregates are summarized in Table 2-1. SiO_2 is the main component in all aggregates. The Si-content in MS as SiO_2 is more than 98% and other components, like K_2O, CaO, Fe_2O_3 and ZnO, are only included in trace amounts. OSSN has an amount of 85.31% of SiO_2 and OSSH of 87.95%. OSSN also contains 6.67% of Al_2O_3, 2.58% of CaO, and traces of Fe_2O_3, TiO_2 and K_2O and OSSH 4.74% of Al_2O_3, 2.55% of CaO, and 2.93% of Fe_2O_3.

Microsilica typically has a grain size between 0.1 and 0.3 µm [27]. The measured diameters in Table 2.1 contradict this. The results of the analysis indicate the typical agglomeration of the MS, which was not possible to break up in distilled water by mixing with an ultrasound treatment. The agglomerated MS in water is clearly visible with a polarization microscope (Leica DM 2500 P) in a 640 x magnification, as seen in Figure 2-2. Figure 2-3 shows the MS directly after blending it with KOH. The incipient separating of the agglomerates is recognizable by the increasing amount of smaller particles. Figure 2-4 presents the MS after 72 hours in KOH. The dissolution of the agglomerates is clearly identifiable. Larger particles like those in Figure 2-2 and Figure 2-3 are no longer available. However, the particles of the sandstones do not tend to agglomerate. Their particle size remains unchanged, even after minutes of ultrasound mixing. The specific surface of OSSN is 51.56 m^2/g and of OSSH 41.42 m^2/g, as seen in Table 2.1. This is nearly three times larger than the specific surface of MS. The reason for this is the larger porosity of opaline sandstone.

Table 2.1: Characterization of the siliceous materials, OSSN and OSSH

	BET	True density	D_{10}	D_{50}	D_{90}	SiO_2	K_2O	CaO	TiO_2	ZnO	Fe_2O_3	Al_2O_3
	[m^2/g]	[g/m^3]		[µm]					[M.-%]			
MS	18.78	2.28	25.48	76.42	98.95	98.95	0.63	0.16	-	0.07	0.19	-
OSSN	51.56	1.48	3.83	35.38	72.05	85.31	1.24	2.58	0.49	-	3.71	6.67
OSSH	41.42	1.69	3.71	24.66	111.33	87.95	2.28	2.55	0.45	-	2.93	4.74

MS has a specific surface of 18.78 m^2/g. The larger BET indicates that the specific surface of the opaline sandstone could result in a faster reaction of the chemical parameter than MS. The numbers of the experiments with equal boundary conditions for MS, OSSN, and OSSH, which are the basis for this paper's investigations, are listed in Table 2.2.

Table 2.2: Numbers of experiments with equal boundary conditions

	3 g	5 g	8 g	10 g	12 g
MS	5	7	4	7	-
OSSN	6	6	-	6	8
OSSH	-	6	-	3	-

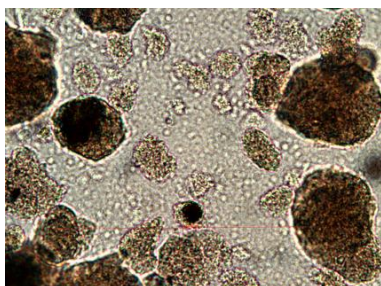
Figure 2.2: MS in water; 640x magnification
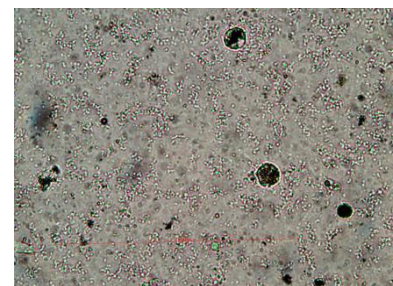
Figure 2.3: MS in KOH; 0 h; 640x magnification

Figure 2.4: MS in KOH; 72 h, 640x magnification

3. RESULTS

3.1 pH-value

Although the pH-value differs for each variation in boundary conditions, noticeable similarities are recognizable in each graphs. The graphs can be divided into four sections, as shown in Figure 3-1. The first section, with the pH-value pH_A, is achieved shortly after reaching the target temperature. Meanwhile, the pH-value decreases to around pH 12.4 due to the increase of the temperatur. Section A is constant until the sample is added at time point zero. pH_A depends up on the experimental temperature and the possible measurement inaccuracy while producing the KOH-solution. After adding the aggregate, the pH-value drops to a significant and global minimum, pH_{min}. The part between point zero and the pH_{min} is called section B. After pH_{min}, the pH rises again in section C until it reaches the last steady state, section D with pH_D. There are different forms of section C. First, the pH-value rises straight after the minimum to section D without significant changes in the slope. Second, there is a short break in the increase of the pH-value. Third, there is another steady state between pH_{min} and pH_D. Figure 3-1 shows the last form of section C for 8 g of OSSN. In section D, the pH_D equals the value of the first steady state, pH_A, and does not change significantly until the end of the experiment. The values of these characteristic points and the form of the sections depend on the quantity and nature of the aggregate.
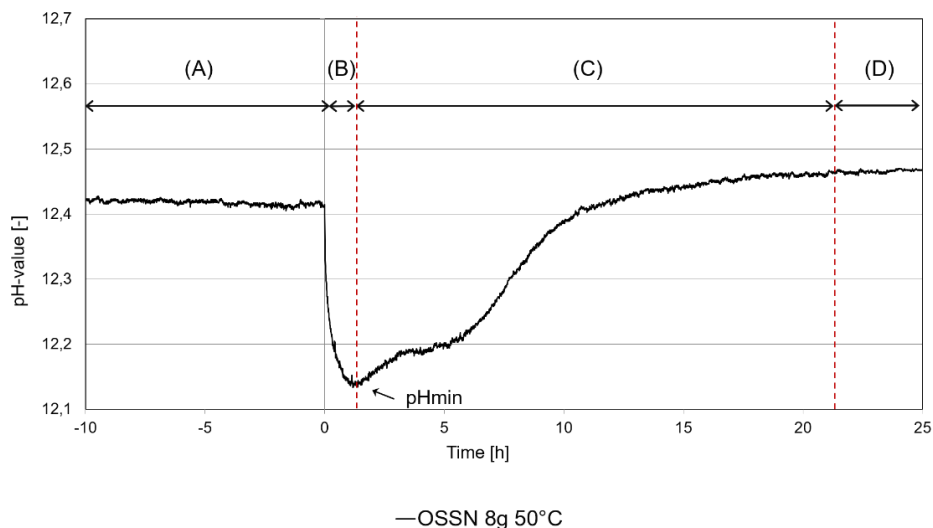

—OSSN 8g 50°C

Figure 3-1: Different sections of pH-value illustrated by 8 g of OSSN

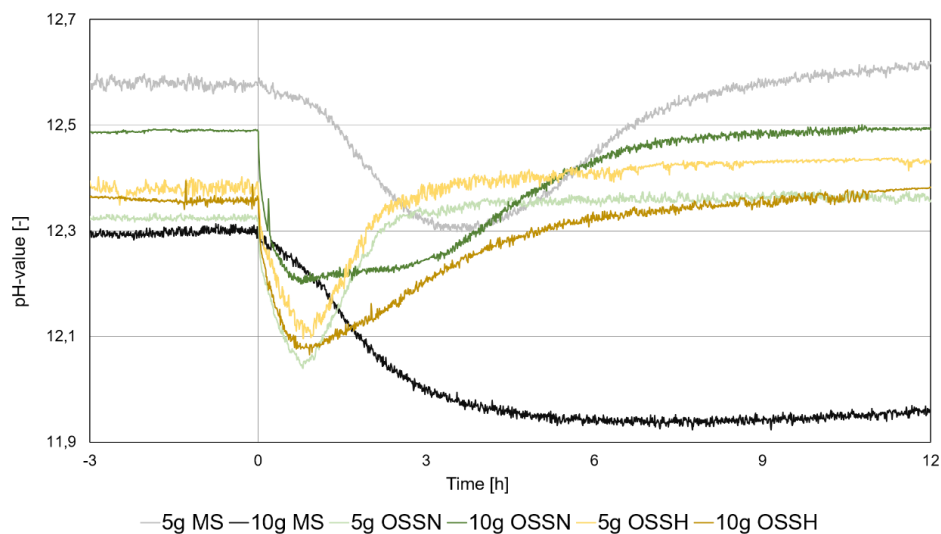—— 5g MS —— 10g MS —— 5g OSSN —— 10g OSSN —— 5g OSSH —— 10g OSSH

Figure 3.2: pH-value vs time for 5 g and 10 g of MS, OSSN and OSSH

In this paper, investigations into sections B and C and the pH_{min} are presented. Regarding the inert quartz powder, the pH-values remain constant throughout the different sections regardless of the amount of the added aggregate [22]. Figure 3-2 presents the pH-value of 5g and 10g of MS, OSSH (both reactiv), and the less reactive OSSN. The different forms of section C are recognizable. Section D for 10 g MS was omitted, for a better scale of diagram.

For the pH_{min}, the minimum is reached earlier for the opaline sandstones than for MS. This can be attributed to the larger specific surface of the opaline sandstones. Moreover, there is a connection between the sample size and the size of the minimum. A larger sample size leads to a more significant reduction of the pH-value. To quantify the drop of the pH, the ratio between the pH_{min} and the pH_A is calculated, as seen in equation (1).

$$Q_{pH,min} = \frac{10^{-pHmin}}{10^{-pHa}}$$

(1)

For a comparison of the different pH-values and for avoiding the influence of background noise, the pH_A is defined as the average pH-value from section A. This results in a representative value, although there are small fluctuations in this state. For pH_{min}, this is insignificant because the minimum is a unique data point. The average value for Q_{pH} (M_{QpH}) over all the experiments with the same boundary conditions, the standard deviation (SD_{QpH}), the variance and the coefficient of variation (CV_{QpH}) are calculated and shown in Table 3.1. The Q_{pH} is calculated with pH-values in a linear scale and a larger Q_{pH} stands for a larger pH-drop. In all cases, M_{QpH} has a tendency to increase with increasing sample size. The CV_{QpH} is smaller or at least 0.140 in all calculations. This reveals a small variation in the data.

Table 3.1: Statistical values of the pH-change after sample addition

[g]	MS			OSSN			OSSH		
	M_{QpH} [-]	SD_{QpH}	CV_{QpH}	M_{QpH} [-]	SD_{QpH}	CV_{QpH}	M_{QpH} [-]	SD_{QpH}	CV_{QpH}
3	1.46	0.20	0.142	1.59	0.14	0.090	-	-	-
5	1.85	0.06	0.036	1.91	0.12	0.063	2.04	0.19	0.095
8	1.99	0.01	0.007	-	-	-	-	-	-
10	2.19	0.04	0.018	2.03	0.27	0.133	2.02	0.09	0.040
12	-	-	-	2.06	0.12	0.060	-	-	-

The relation between the sample size and the M_{QpH} of one type of aggregate and its standard deviations M_{QpH} - SD_{QpH} and M_{QpH} + SD_{QpH} are illustrated in Figure 3-3. For MS (black lines) and OSSH (brown lines), the M_{QpH} increases clearly with the sample size. This contrasts to OSSN (green lines), which seems to reach a limit for M_{QpH} after a certain sample size. This is a difference to the other more reactive samples which is not distinguishable in the investigated sample sizes of the more reactive samples. The comparison of the different and more reactive aggregates shows that the drop in MS pH-value is always slightly larger than for OSSH. For a sample size smaller than 8 g, the pH-drop of MS is even smaller than the less reactive OSSN. The reason for this is not clear. It could be attributed to the different size of the surface areas in conjunction with the reachability and amount of dissolvable SiO_2 in the sample. There is no general relation between the different samples for the same sample sizes.
Figure 3.4 shows the duration and its standard deviations in minutes until the pH_{min} of MS, OSSN and OSSH is reached. The time periods are the averages over all the experiments with the same boundary conditions according to the different aggregates. For MS, the duration increases with increasing sample size, reaches a maximum duration at a sample size of 8 g and decreases again. In case of 3 g of MS, the standard deviations is 30%. Thus, it is not clear whether the time until the pH_{min} is reached, increasing linearly with the sample size. Taking a look at the opaline sandstone, the duration for reaching the pH_{min} seems to be constant, and not attached to the sample size. It takes 50 minutes until pH_{min} is reached. For 10 g of OSSN, it takes 100 minutes. Here, the standard deviation is 40 minutes. This data point might thus be an outlier, and can be disregarded. It is striking that the pH_{min} is reached significantly faster in the OSSN and the OSSH. This is independent of the amount of the aggregate and caused by the larger specific surface of the opaline sandstone. It seem that 50 minutes is a characteristic duration for reaching the pH_{min} for opaline sandstone.
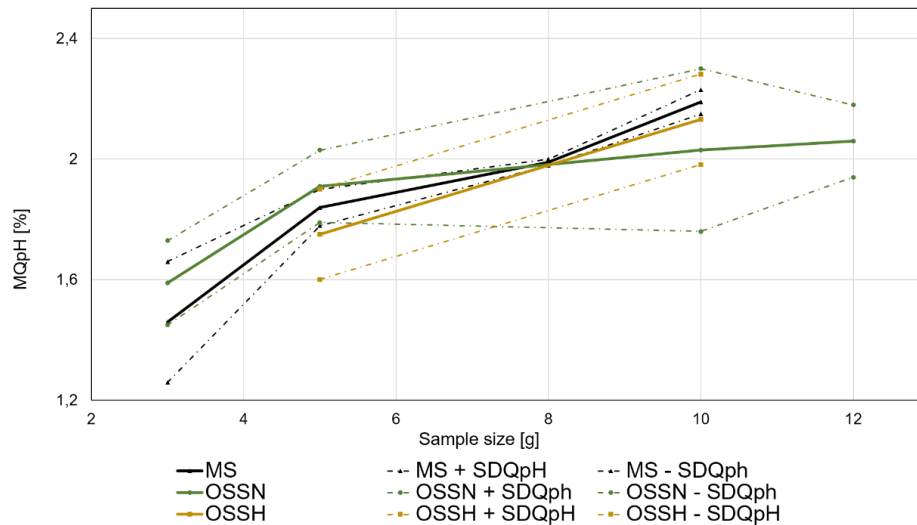
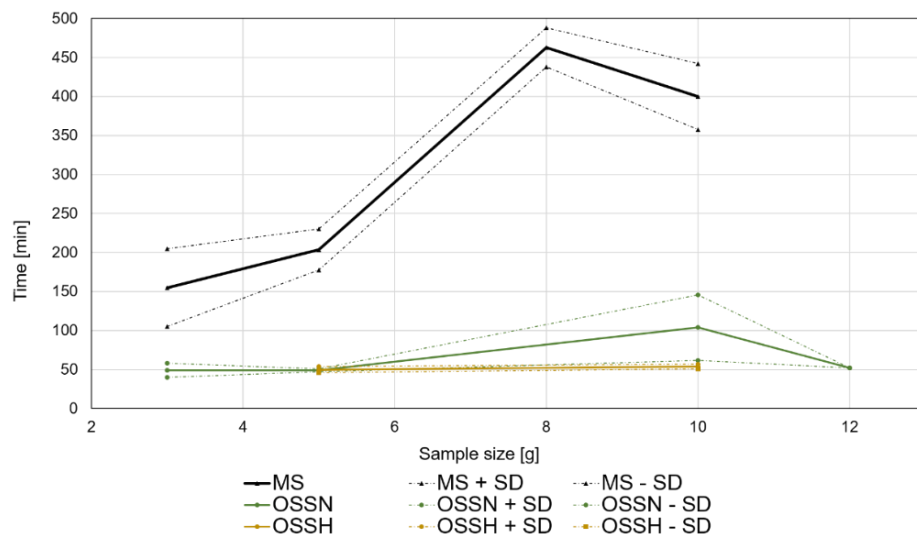Figure 3.3: pH-change; statistical values compare to Table 3.1

Figure 3.4: Period [min] until the pHmin is reached, for different sample size of MS, OSSN, and OSSH

The different forms in section C depend on the sample size and the type of the aggregate. For a small sample size, the pH-value increases without changing the slope to the next section. A larger sample size causes a change in the slope, and an even larger sample size causes a second steady state in this section. The critical sample size which changes section C decreases along with the alkali-reactivity of the aggregate.

3.2 Electrical conductivity

The graphs of the electrical conductivity are divided into three sections, as shown in Figure 3.5. The first section, section A with LF_A, ends by adding the aggregate. The electrical conductivity is constant in this section and depends on the experimental temperature. In section B, the conductivity decreases until it is constant again in the third section, section C. In section C, the conductivity (LF_C) does not change significantly for the further duration of the experiment. Figure 3.5 presents the sections through the example of 10 g MS.

In this paper, the relation between the constant sections A and C are presented. Adding the inert quartz powder does not change the electrical conductivity (LF). The values remain constant within all sections [22]. For quantifying the difference between LF_A and LF_C the ratio (Q_{LF}) is calculated. LF_A and LF_C are the averages of data points from the respective sections for minimizing the background noise.
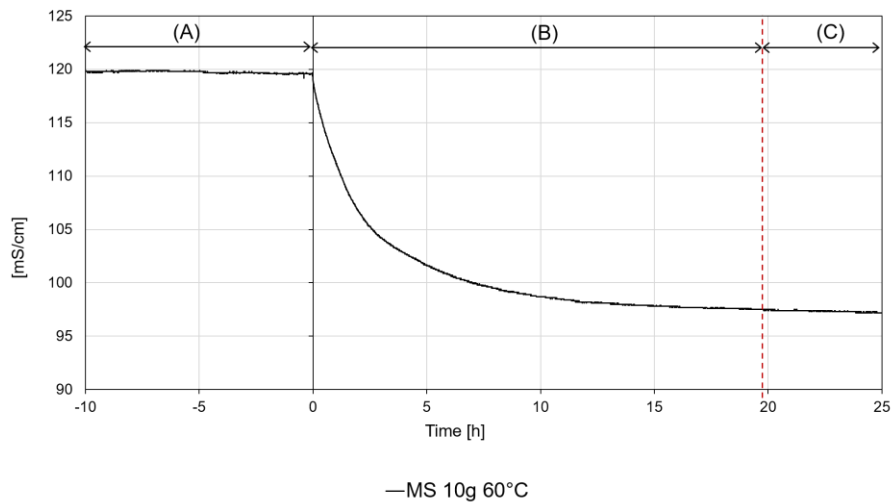
—MS 10g 60°C

Figure 3.5: Different sections of LF illustrated by 10 g of MS

The average value for Q_{LF} (M_{QLF}) over all the experiments with the same boundary conditions, the standard deviation (SD_{QLF}), the variance and the coefficient of variation (CV_{QLF}) is shown in Table 3.2. The CV_{QLF} for all the experiments, with the exception of 5 g of OSSH, shows a small variance in value, indicating a good reproducibility of results. For MS, the M_{QLF} clearly decreases with the amount of aggregate. It reaches a minimum at 8 g of MS and rises again.

Table 3.2: Statistical values of the LF-change after sample addition

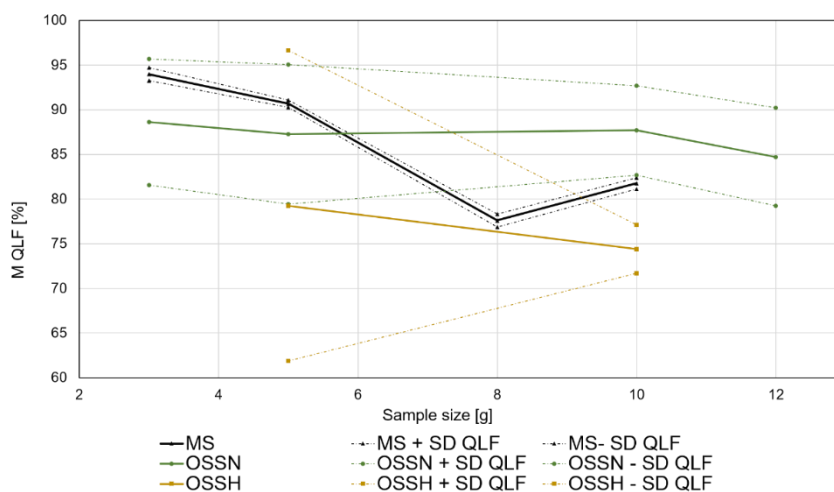|	MS			OSSN			OSSH		
[g]	M_{QLF} [%]	SD_{QLF}	CV_{QLF}	M_{QLF} [%]	SD_{QLF}	CV_{QLF}	M_{QLF} [%]	SD_{QLF}	CV_{QLF}
3	94.00	0.71	0.008	88.65	7.07	0.080	-	-	-
5	90.69	0.41	0.004	87.27	7.82	0.090	79.25	17.40	0.220
8	77.62	0.73	0.009	-	-	-	-	-	-
10	81.76	0.63	0.008	87.69	4.99	0.057	74.40	2.71	0.036
12	-	-	-	84.73	5.49	0.065	-	-	-

Figure 3.6: LF-change; statistical values compare to Table 3.2

For OSSN, the conductivity decreases slightly with the sample size. LF_B is between 88.65% and 84.73% of LF_A. Regarding the standard deviation, this could interpreted as constant. For OSSH, the slope of the

M_{QLF} is larger. However, the wide standard deviation of 22% regarding 5 g of OSSN impedes a clear statement, whether an increase of the sample size leads to a decrease of the M_{QLF}.

The relation between the sample size and the M_{QLF} is shown in Figure 3.6. M_{QLF}, M_{QLF} - SD_{QLF} and M_{QLF} + SD_{QLF} are shown against the sample size. The comparison of the three samples shows a change in relation between sample size and decrease in M_{QLF}. The enlargement of alcali-reactivity increases the influence of the sample size on the increase of M_{QLF}. Thus less reactive aggregates lead to a smaller slope of the M_{QLF} despite a larger sample size.

3.3 Redox potential

The redox potential is more irregular than the pH-value or the electric conductivity. Despite these irregularities, it is dividable into four sections, as shown in Figure 3.7. The first section, section A (RD_A), ends by adding the aggregate at time point zero. The redox potential differs in this section from experiment to experiment irrespective of whether the boundary conditions are equal or not. RD_A could be constant, increase or decrease. Despite the various courses of RD_A, the addition of the aggregate leads to a sharp drop in the redox potential and a global minimum, RD_{min}. In the third section, section C the redox potential increases clearly until it reaches a limit RD_D and the last section, section D. In section D, RD_D can accommodate a constant value or it can reach a local maximum and decrease slightly afterwards, until the experiment ends. In both cases, the constant RD_D and the local maximum are lower than the last value of section A. The graph of the redox potential caused by the inert quartz powder shows a continuous increase of values, independent of adding the aggregate [22].

The RD_{min} is investigated in this paper. Its average M_{RDmin}, its standard deviation SD_{Rdmin} and the absolute value of the coefficient of variation CV_{RDmin} are shown in Table 3.3. The large standard deviations lead to the assumption that there is no obvious relation between the amount of the aggregate and the respective M_{Rdmin}. The M_{RDmin} of one aggregate does not differ significantly regarding the different quantities of the sample. The average of RD_{min}, neglecting the different sample sizes, indicates a minimum, independent of the sample size but dependent on the nature of the sample. A less reactive sample leads to a smaller RD_{min}.
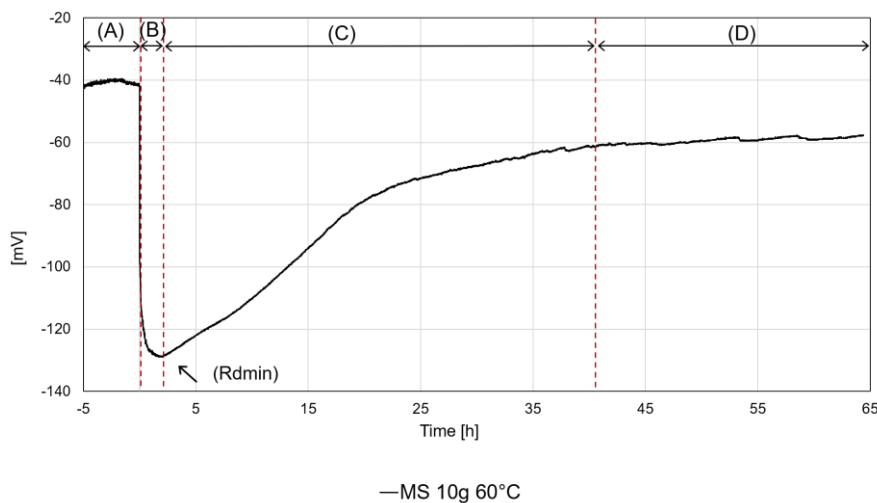

Figure 3.7: Different sections of redox potential illustrated by 10 g of MS

Table 3.3: Statistical values of the *RDmin* after sample addition

[g]	MS			OSSN			OSSH		
	M_{RDmin}	SD_{RDmin}	CV_{RDmin}	M_{RDmin}	SD_{RDmin}	CV_{RDmin}	M_{RDmin}	SD_{RDmin}	CV_{RDmin}
3	-118.87	10.59	0.088	-103.75	6.67	0.065	-	-	-
5	-131.75	13.86	0.105	-99.57	11.83	0.114	-127.40	9.36	0.074
10	-131.73	14.13	0.107	-115.07	8.56	0.074	-131.93	9.85	0.075
Total	-128.06	13.79	0.108	-106.43	11.28	0.106	-130.86	11.28	0.086

4. SUMMARY, CONCLUSION, OUTLOOK

A new, direct, rapid method for testing the interaction of aggregates with a synthetic concrete pore solution was presented here. The preparation of the material and the experimental setup were described, and first results were shown. The first general results are the reproducibility of the data and the reliable division of the values into different sections. Further results are:

pH-value:

- A drop in pH reaches a limit, independent of the sample size for less reactive aggregates.
- A drop in pH increases with increasing sample size for reactive aggregates.
- The duration until pH_{min} is reached is independent of the sample size, and constant for opaline sandstone.

Electrical conductivity:

- The conductivity drop increases with the sample size.
- This increase is smaller for less reactive aggregates.

Redox potential:

- RD_{min} is independent of the sample size and characteristic for certain aggregates.

To improve the accuracy of the characteristics and to collect the characteristics of different aggregates, further studies must be done. More investigations are required to determine the kinetic aspect of the redox potential, the pH-value and their relation to the amount and characteristics of the aggregate.

5. REFERENCES

[1] Alexander, G. B., Heston, W. M., and Iler, R. K. 1954. The Solubility of Amorphous Silica in Water. *J. Phys. Chem.* 58, 6, 453–455.

[2] Alexander, M. G. and Mindess, S. 2008. *Aggregates in concrete*. Modern concrete technology series v. 13. Taylor & Francis, London, New York.

[3] Amjad, Z., Ed. 2014. *Mineral scales in biological and industrial systems*. CRC Press, Boca Raton, Fla.

[4] Bickmore, B. R., Wheeler, J. C., Bates, B., Nagy, K. L., and Eggett, D. L. 2008. Reaction pathways for quartz dissolution determined by statistical and graphical analysis of macroscopic experimental data. *Geochimica et Cosmochimica Acta* 72, 18, 4521–4536.

[5] Bulteel, D., Garcia-Diaz, E., Vernet, C., and Zanni, H. 2002. Alkali–silica reaction. *Cement and Concrete Research* 32, 8, 1199–1206.

[6] C09 Committee. *Test Method for Determination of Length Change of Concrete Due to Alkali-Silica Reaction*. ASTM International, West Conshohocken, PA.

[7] C09 Committee. *Test Method for Potential Alkali Reactivity of Aggregates (Mortar-Bar Method)*. ASTM International, West Conshohocken, PA.

[8] Crundwell, F. K. 2017. On the Mechanism of the Dissolution of Quartz and Silica in Aqueous Solutions. *ACS omega* 2, 3, 1116–1127.

[9] 2013. *DAfStb-Richtlinie Vorbeugende Maßnahmen gegen schädigende Alkalireaktion im Beton : (Alkali-Richtlinie)*. DAfStb-Richtlinie. Dt. Ausschuss für Stahlbeton, Berlin.

[10] Dove, P. M., Han, N., Wallace, A. F., and Yoreo, J. J. de. 2008. Kinetics of amorphous silica dissolution and the paradox of the silica polymorphs. *Proceedings of the National Academy of Sciences of the United States of America* 105, 29, 9903–9908.

[11] Eikenberg, J., Paul-Scherrer-Institut, and Nationale Genossenschaft für die Lagerung Radioaktiver Abfälle. 1990. *On the Problem of Silica Solubility at High PH*. PSI-74. Paul Scherrer Institut.

[12] Fernandes, I. and Broekmans, M. A. T. M. 2013. Alkali–Silica Reactions: An Overview. Part I. *Metallogr. Microstruct. Anal.* 2, 4, 257–267.

[13] Franke, L. 2002. *Schnelltest auf Alkalireaktion für deutsche Beton-Zuschläge. [Forschungsbericht].* Bau- und Wohnforschung F 2419. Fraunhofer-IRB-Verl., Stuttgart.

[14] Giebson, C. 2013. *Die Alkali-Kieselsäure-Reaktion in Beton für Fahrbahndecken und Flugbetriebsflächen unter Einwirkung alkalihaltiger Enteisungsmittel.* Dissertation, Bauhaus-Universität Weimar.

[15] Goto, K. 1956. Effect of pH on Polymerization of Silicic Acid. *J. Phys. Chem.* 60, 7, 1007–1008.

[16] Greenberg, S. A. 1957. The Depolymerization of Silica in Sodium Hydroxide Solutions. *J. Phys. Chem.* 61, 7, 960–965.

[17] Helmuth, R. A. 1993. *Alkali-silica reactivity. An overview of research.* Strategic Highway Research Program, National Research Council, Washington, DC.

[18] Iler, R. K. ca. 2004. *The chemistry of silica. Solubility, polymerization, colloid and surface properties, and biochemistry.* Wiley, New York, NY.

[19] *Kaliumhydroxid 85.0-100.5%, Plätzchen Ph. Eur.* https://de.vwr.com/store/product/2376850/ kaliumhydroxid-85-0-100-5-platzchen-ph-eur. Accessed 13 February 2020.

[20] Mehta, P. K. and Monteiro, P. J. M. 2014. *Concrete. Microstructure, properties, and materials.* McGraw-Hill's AccessEngineering. McGraw-Hill Education, New York.

[21] Oberholster, R. E. and Davies, G. 1986. An accelerated method for testing the potential alkali reactivity of siliceous aggregates. *Cement and Concrete Research* 16, 2, 181–189.

[22] Osterhus, L., Dombrowski, C., and Schmidt-Döhl, F. 2015. *Löslichkeitsuntersuchungen zur schnellen Beurteilung der Alkalireaktivität von Gesteinskörnungen.* Internationale Baustofftagung, Weimar.

[23] Osterhus, L. and Schmidt-Döhl, F. 2014. Verbessertes Prüfverfahren zur Beurteilung der Alkalireaktivität von Gesteinskörnungen basierend auf Lösungsversuchen. In *GDCh-Monographie Band 48. Tagung Bauchemie 2014.* Gesellschaft Dt. Chemiker, Frankfurt am Main, S. 41-44.

[24] Rajabipour, F., Giannini, E., Dunant, C., Ideker, J. H., and Thomas, M. D.A. 2015. Alkali–silica reaction: Current understanding of the reaction mechanisms and the knowledge gaps. *Cement and Concrete Research* 76, 130–146.

[25] Ramos, V., Fernandes, I., Santos Silva, A., Soares, D., Fournier, B., Leal, S., and Noronha, F. 2016. Assessment of the potential reactivity of granitic rocks — Petrography and expansion tests. *Cement and Concrete Research* 86, 63–77.

[26] Stanton, T. E. 1940. Expansion of concrete through reaction between cement and aggregate. *American Society of Civil Engineers,* 66(10) (Dec. 1940), 1718–1811.

[27] Stark, J. and Wicht, B. 2013. *Dauerhaftigkeit von Beton.* Springer Berlin Heidelberg, Berlin, Heidelberg.

[28] Swamy, R. N., Ed. 2003. *The alkali-silica reaction in concrete.* The Taylor & Francis e-Library. Blackie and Son, Glasgow.

[29] Thomas, M. D.A., Fournier, B., Folliard, K. J., and Transtec Group, I. 2013. *Alkali-aggregate Reactivity (AAR) Facts Book.* Federal Highway Administration, Office of Pavement Technology.

[30] Visser, J.H.M. 2018. Fundamentals of alkali-silica gel formation and swelling: Condensation under influence of dissolved salts. *Cement and Concrete Research* 105, 18–30.